Examining Urban Heat Island Relations to Land Use and Air Pollution: Multiple Endmember Spectral Mixture Analysis for Thermal Remote Sensing

Bakhtiar Feizizadeh and Thomas Blaschke

***Abstract*—This paper proposes an integration of Spectral Mixture Analysis and Endmember Remote Sensing Indices to derive land surface temperature (LST), to identify urban heat islands (UHI) and to investigate their relationships to land use/land cover (LULC) and air-pollution in Tabriz city, Iran. LST values are assessed from ASTER remotely sensed thermal images to appraise the intensity of UHIs through a statistical approach. The results indicate that LST is highly influenced by LULC and that UHIs are closely linked to LST and LULC. As expected, LST is sensitive to vegetation and moisture and low temperatures are found in water bodies and vegetated areas. High temperatures are related to construction zones and industrial sites which are not necessarily located in the city centre. While the results demonstrate a high correlation between UHIs and air-pollution spatial analysis discloses a different pattern: when correlating identified UHI zones with air pollution the market area of Tabriz city reveals the highest measured PM values.**

***Index Terms*—Air pollution, ASTER, endmember remote sensing indices, land surface temperature, land use, spectral mixture analysis, Tabriz city, urban heat island.**

I. Introduction

URBAN heating and the formation of urban heat islands (UHIs) is one attribute of urban land transformation that is of interest across science disciplines, since the UHI signal reflects a broad suite of important land surface changes impacting human health, ecosystem function, local weather and, possibly, climate [1]. In recent years, the mapping of urban biophysical and thermal conditions, as well as their relation to land use and land cover (LULC) and air pollution, has attracted increasing interest. In most cases, UHIs are a result of the use of fossil fuels which affects air-pollution in urban areas. It is a well-known fact that increasing population numbers, particularly in developing countries, intensify the pressure on natural resources [2]. Rapid population growth, in conjunction with urbanization, expansion, and encroachment into the limited agricultural and green areas lead to the destruction of vegetation coverage [3]. It is obvious that such destruction, in combination with population growths, causes environmental impacts such as intensified land surface temperature (LST), UHIs and air-pollution. LST is considered as one of the important parameters in urban climate, which directly controls the UHI effect. LST is believed to correspond closely with the LULC, resulting in heat islands [4]. LST research shows that the balance of land surface energy can be influenced by the conversion of surface soil, water content, and vegetation [5]. It is well known that the incoming and outgoing radiation of urban surfaces correspond closely to the distribution of LULC characteristics [6], [7]. An increasing number of studies analyse urban climate and, in particular, differences in observed ambient air temperature between cities and their surrounding rural regions, which collectively describe the UHI effect [4], [8]. A wide range of satellite and airborne sensors—including thermal sensors—have been used to study UHIs [3]. In general, thermal remote sensing is regarded as an efficient technology which provides a synoptic and uniform means of studying UHI effects on a regional scale. In the absence of a dense network of land-based meteorological stations, the spatiotemporal distribution of LSTs from thermal remote sensing imagery can be used as information to support UHI management [9] and, potentially, countermeasures. Thermal satellite measured LST has been utilized in various heat-balance, climate modelling, and global change studies since it is determined by the effective radiating temperature of the Earth's surface, and to assess UHIs [10]. LST is also used in models of land surface atmosphere exchange, and when analyzing the relationship between temperature and LULC [11], [3]. Based on this idea, the main objective of this research is to investigate the relationship between LST, UHI and LULC in Tabriz city, using ASTER thermal remote sensing satellite images.

II. Study Area and Data

The study area of Tabriz city is located in Northwestern Iran. Tabriz city has about 2 million inhabitants and is one of the most important urban and industrial regions in Iran. Tabriz has a semi-arid climate with pronounced seasons. The temperature varies between $+38\,\mathrm{C}^{\circ}$ and $-15\,\mathrm{C}^{\circ}$. The city is almost entirely surrounded by the steep foothills of mountain ranges [3]. The topographical situation and the increasing number of industrial sites lead to a growing UHI effect, as well as to rising air pollution.

In order to obtain LST and subsequently UHI zones, ASTER images were acquired for June 25, 2011. ASTER is one of the major satellite sensors used for LST and UHI determination [12]. In our research, the separate bands were layer stacked and

Manuscript received March 20, 2013; accepted May 11, 2013. Date of publication May 30, 2013; date of current version June 17, 2013. This work was supported in part by the Austrian Science Fund (FWF) through the Doctoral College GIScience (DK W 1237-N23).

B. Feizizadeh is with the Center for GIS and Remote Sensing, Department of Physical Geography, University of Tabriz, Tabriz 51368, Iran. He is also with the Department of Geoinformatics, University of Salzburg, Salzburg 5020, Austria (corresponding author, e-mail: feizizadeh@tabrizu.acir; bakhtiar.feizizadeh@stud.sbg.ac.at).

T. Blaschke is with the Department of Geoinformatics, University of Salzburg, Salzburg 5020, Austria (e-mail: Thomas.Blaschke@sbg.ac.at).

Color versions of one or more of the figures in this paper are available online at http://ieeexplore.ieee.org.

Digital Object Identifier 10.1109/JSTARS.2013.2263425

transformed to pixel sizes of 15 by 15 m, in order to preserve the spatial features provided in the VNIR bands. Then the atmospheric correction was carried out using ENVI software. In terms of the geometric correction, digital topographic maps of 1:25,000 scale and GPS based ground control points were used to correct the images. In order to achieve an acceptable geometric accuracy, 25 ground control points were used. A polynomial model was used for the rectification process with nearest neighbor resampling. The root-mean-square-error (RMSE) of the images was estimated to be 0.38.

III. Methods

A. Remote Sensing Indices Used

First, original ASTER digital numbers (DNs) were converted to radiance values. The visible and near-infrared bands were transformed to reflectivity values and the thermal infrared bands to radiant brightness values, using the parameters provided in the header file. Respectively, the radiant brightness was converted to the brightness temperature based on the Planck function. In order to obtain accurate LST values, we adopted the subpixel temperature approach based on the endmember remote sensing indices (DisEMI). As the base of the DisEMI technique, the selection of remote sensing indices plays an important role when estimating subpixel temperature for different land cover types [13]. ASTER data provide a total of 9 VNIR/SWIR wavebands which can be selected when constructing different remote sensing indices for different land cover types based on the difference of spectral characteristics. We used the disTrad and the TsHARP techniques [13], [14]. The NDVI-LST relationship exists within a sensor scene at multiple spatial resolutions. Similarly, in order to predict LST from available ASTER bands, the normalized difference spectral indices (NDSI) were employed with "pure pixels" temperature for each land cover type [13]:

$$NDSI_{(x,y)} = \frac{r_x + r_y}{r_x + r_y} \quad (1)$$

where r is the reflectance; x and y represent the central wavelength of each ASTER VNIR/SWIR band.

The normalization aims to reduce atmospheric or other sources of disturbances, reducing the proportional changes of the reflectance spectrum, as well as enhancing the spectral response to observed targets [13], [15]. In this study, all combinations of the nine ASTER VNIR/SWIR bands were applied in the NDSI formula as described in [13].

B. Linear Spectral Mixture Analysis

In order to extract subpixel information a linear spectral mixture analysis (LSMA) approach was performed. LSMA is a physically based image processing technique, which supports a repeatable and accurate extraction of quantitative subpixel information [16], [17]. It is believed that the spectrum measured by a sensor is a linear combination of the spectra of all components within the pixel [18]. Because of its effectiveness in handling the spectral mixture problem, LSMA has been widely used in urban UHI studies [18], [19]. LSMA provides subpixel endmember fraction estimates, probably the most commonly used technique of all subpixel analysis techniques. An endmember is the spectrum of a pure ground component (e.g., vegetation, soil, water) and thus LSMA endmember fractions are typically interpreted as ground component fractions [20]. The LSMA approach can be mathematically expressed as follows [20]:

$$Xi = \sum_{k=1}^{n} f_k X_{\mathrm{ik}} + e_i \quad (2)$$

where $X_i =$ spectral reflectance of pixels in band i, $n =$ number of endmembers, $f_k =$ fraction of endmember k within a pixel, $X_{\mathrm{ik}} =$ known spectral reflectance of endmember k within the pixel in band i, and $e_i =$ error term for band i [22]. In respect to (2), lowest root mean square error (RMSE) can be computed as follows [20]:

$$\mathrm{RMSE} = \left[\frac{\sum_{j=1}^{m} (e_{ij})2}{m} \right]^{0.5} \quad (3)$$

where e_i is the error term for each of the m spectra considered. Applying LSMA to remotely sensed satellite imagery typically also adds the following additional constraints [20]:

$$\sum_{k=1}^{n} f_k = 1 \text{ and } 0 \leq f_k \leq 1. \quad (4)$$

Because finding f_k requires solving a system of m or $m+1$ (when the sum of fractions is forced to be 1) equations, the number of endmembers cannot exceed the number of bands m [20]. Since ASTER imagery contains nine VNIR and SWIR bands and five TIR bands, both the urban biophysical descriptors and thermal features can be extracted from them. These image transformations would allow the relationship between LST and biophysical descriptors to be examined [16].

C. Multiple Endmember Spectral Mixture Analysis

Numerous variants of LSMA have been developed to address the issue of endmember variability. In this regard, Multiple Endmember Spectral Mixture Analysis (MESMA) was developed by Roberts *et al.* [21] to allow the number and type of endmembers to vary on a per-pixel basis [22]. MESMA iteratively computes linear models using different sets of endmembers, and the model with the lowest RMSE is selected for each individual pixel [22]. In practice, MESMA iteratively computes linear models using different sets of endmembers, and the model with the lowest RMSE is selected for each individual pixel [22]. The flexibility of MESMA has permitted its application to mapping a wide variety of vegetated and non-vegetated land cover. Within this research the advantage of MESMA together with NDSI and LSMA was used to retrieve LST and subsequently to identifying UHI zones.

D. Computing Land Surface Temperature

In order to compute LST as a base map for UHIs we selected ASTER band 13 (10.25–10.95 μm), since the spectral width of this band is close to the peak radiation of the black-body spectrum released by the urban surface of the study area. Two steps must be considered when computing LSTs from ASTER satellite images: 1) spectral radiance must be converted to at-sensor brightness temperature (i.e., black-body temperature); and

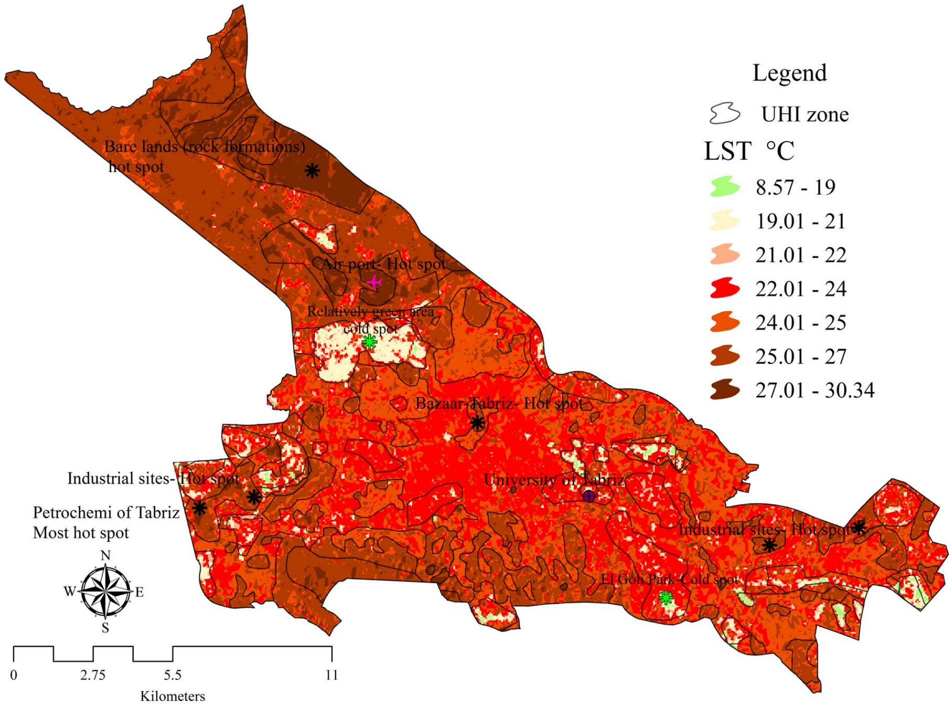

Fig. 1. Spatial distribution of the derived LST and the identified UHI zones in Tabriz city.

2) spectral emissivity must be corrected [16]. We adopted the most straightforward approximation of replacing the sensor response function with a delta function at the sensor's central wavelength, to invert LSTs with the assumption of uniform emissivity [23], [16]. The conversion performed is based on the following equation [16]:

$$T_c = \frac{C_2}{\lambda_c 1n\left(\frac{C_1}{\lambda_c^5 \pi L_\lambda} + 1\right)} \tag{5}$$

where T_c is the brightness temperature of the central wavelength in Kelvin (K), L_λ is the spectral radiance in $\mathrm{Wm}^{-3}\mathrm{sr}^{-3}\mu\mathrm{m}^{-1}$, λ_c is the sensor's central wavelength, C_1 is the first radiation constant ($3.74151 * 10^{-16}$ $\mathrm{Wm}^{-3}\mathrm{sr}^{-3}\mu\mathrm{m}^{-1}$) and C_2 is the second radiation constant ($0.0143879\ \mathrm{m \cdot k}$). The temperature values obtained above are in reference to a black body. Therefore, a correction of spectral emissivity (ε) became necessary in regard to the nature of land cover [16]. In this regard, Snyder *et al.* [24] assigned an emissivity value to each of the land cover categories according to an emissivity classification scheme. The emissivity-corrected LSTs were computed as follows [16]:

$$\mathrm{LST} = \frac{T_c}{1 + \left(\lambda * \frac{T_c}{p}\right) 1n\varepsilon}. \tag{6}$$

where λ = wavelength of emitted radiance (the peak response and the average of the limiting wavelengths) [$\lambda = 10.6\ \mu$m]. $p = \mathrm{h} * \mathrm{c}/\sigma$ ($1.438 * 10^{-2}$ m · K), σ = Boltzmann constant ($1.38*10^{-23}\ \mathrm{JK}^{-1}$), h = Planck's constant ($6.626*10^{-34}$ J·s) and c = velocity of light ($2.998 * 10^8\ \mathrm{ms}^{-1}$) [16].

E. Selection of Endmembers

In LSMA, the spectral signatures of the mixed pixels are assumed to be a linear combination of the spectral signatures of the surface materials which are known as endmembers, components or cover types, with their areal proportions as weighting factors [25]. Selection of the endmembers is a critical step, as development of high-quality fraction images depends strongly on the selection of suitable endmembers [26] which is considered to be the key to success in LSMA and MESMA application [25].

There are several advantages in using endmembers. Firstly, they contain the same systematic errors due to atmospheric correction as the image to be unmixed [20]. Secondly, the endmembers can represent responses from the selected material at the same scale as the original image [20]. The selection of image endmembers can be effectively performed through the use of a pixel purity index (PPI) [27], [20]. The PPI method calculates a score for each pixel, based on the number of times it is found to occupy a near-vertex position in the repeated projections of the n-dimensional data onto a randomly oriented vector passing through the mean of the data cloud. The output scores help identify image endmembers, since the pixels that hold pure spectra often display high PPI scores [20].

For calculating endmembers in our study, ENVI software was used. We selected endmembers manually by visualizing the PPI results of spectrally pure pixels, which are identified using the PPI in an n-dimensional visualizer. The image-based endmember selection approach was applied to identify two categories of endmembers (i.e., cold object and hot object). In order for this to happen, the TIR bands were used to identify five endmembers from the VNIR and SWIR bands. The regions of interest determined for the endmembers, defined in the maximum noise fraction feature spaces, were used to extract endmembers' spectra from the calibrated 9-band ASTER imagery using a common spectral unmixing method [27], [20].

F. Extraction of Thermal Features Using LSMA and MESMA

In order to integrate ASTER's five TIR bands into a new dataset, principal component analysis (PCA) was used. PCA is used here for the integration of the main information of the five thermal bands into the LST calculation. In this respect, the PCA is used to convert TIR bands into new datasets, and the outcome of PCA can be used to identify the number of endmembers. The urban environment was assumed to be composed of three fundamental components, namely vegetation (mainly green vegetation), impervious and soil. The impervious component in urban environment includes artificial surfaces which vary widely in spectral response. Two main categories of impervious surface components were assumed: a high-albedo and a low-albedo component [16]. Bright impervious surface information is included in the high-albedo component while dark impervious surface information is included in the low-albedo component [26]. Respectively, the hot- and cold- object endmembers were selected based on the scatterplots between the TIR images. The hot-object endmember represented objects with high thermal radiance such as industrial sites, and the cold-object endmember represented objects with low thermal radiance such as water bodies and green spaces area. A constrained least-squares solution was then applied to unmix the five TIR bands into hot-object and cold-object fraction images. The hot-object fraction image displayed high values in industrial areas, medium values in residential areas, construction sites and bare lands, and low values in green lands and water bodies. The derived LST map represents the LST values range between 8 and 30°C (see Fig. 1).

G. Correlating LST and NDVI

The relationship between LST and vegetation cover has been frequently studied using vegetation indices such as the NDVI [16] which provides an estimate of the abundance of actively photosynthesizing vegetation. In this study, NDVI was calculated for the ASTER images used. It is well known that higher NDVI values typically indicate a larger fraction of vegetation in a pixel. The amount of vegetation determines the LST by the latent heat flux from the surface to atmosphere via evapotranspiration. Lower LSTs are usually found in areas with high NDVI. This negative correlation between NDVI and LST is valuable for urban climate studies [2]. Within our study, the NDVI was used to examine the relationship between LST and vegetation cover. NDVI values for each pixel were scaled between bare soil ($NDVI_0$) and dense vegetation ($NDVI_S$) within a given scene. The scaled value was calculated as follows [3]:

$$N^* = \frac{(NDVI - NDVI_0)}{(NDVI_S - NDVI_0)}. \tag{7}$$

Using the scaled $NDVI(N^*)$, the fractional vegetation cover (Fr) was calculated:

$$\mathrm{Fr} = N^{*2}. \tag{8}$$

This nonlinear relationship was based on the assumption of unstressed vegetation conditions [27]. Temperature values were also scaled between the minimum and maximum values. These values were identified in the LST image, and were used to calculate the normalized temperature values as follows [3]:

$$T^* = \frac{(T_\mathrm{s} - T)_0}{(T_{\max} - T_0)} \tag{9}$$

where T_s is the LST for a given pixel, T_0 is the minimum temperature value corresponding to dense vegetation, and $T_{\max}$ is the maximum temperature value corresponding to bare soil, all obtained within a given scene [3]. The detailed results and correlation coefficients between LST, NDVI, and LULC are presented in Table I.

TABLE I
CORRELATION COEFFICIENTS BETWEEN LST, NDVI, AND LULC

LULC	Correlationcoefficients
River &water bodies	-0.27
Green lands	0.71
Bare lands	0.46
Airport	-0.69
Under construction	0.84
Market area	-0.70
Industry area	-0.74
Constructed area	-0.78

H. Calculation of UHI Intensity

Once the LST is obtained, the UHI intensity can be calculated respectively [20]. At the micro-scale, the UHI intensity was strongly influenced by pixels with extreme LST values [18]. In order to investigate the sensitivity of urban temperature analysis and measurement of the UHI in respect to temporal averaging, statistical comparisons were performed for several levels of aggregation. To examine the spatial distribution of surface radiant temperatures, the LST map was reclassified into seven temperature zones based on the classification scheme of standard deviation. These classes were differentiated based on the mean and standard deviation of the data distribution. The averaged LSTs of those five areas were regarded as the comparable temperature in Tabriz city. Fig. 1 depicts the spatial distribution of identified UHI zones.

I. Relationship Between UHIs and Air-Pollution Maps

In order to compare UHIs and air-pollution conditions, ground-based measurements of particular matter (PM) were obtained on same day as the ASTER satellite images (June 25, 2011). The PM data was recorded by eight ground-based air-pollution measurement stations within different parts of Tabriz city. The results of this data were interpolated using the inverse distance weighted method in GIS. In the following step, the PM map was compared to UHI zones. Fig. 2 shows the resulting spatial distribution for the PM data in Tabriz city.

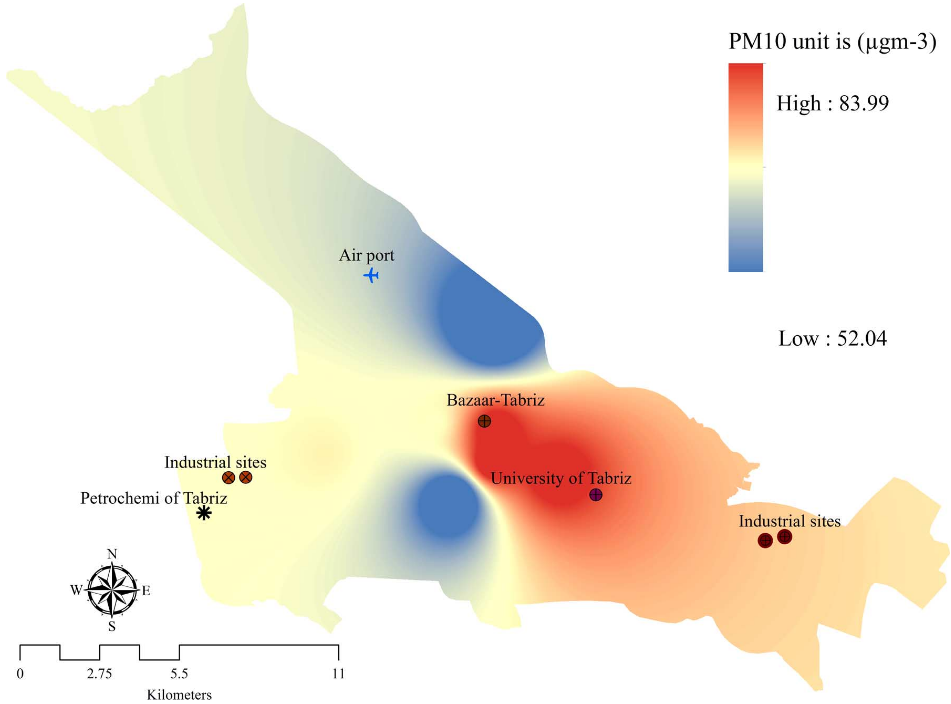

Fig. 2. Air pollution map of Tabriz city.

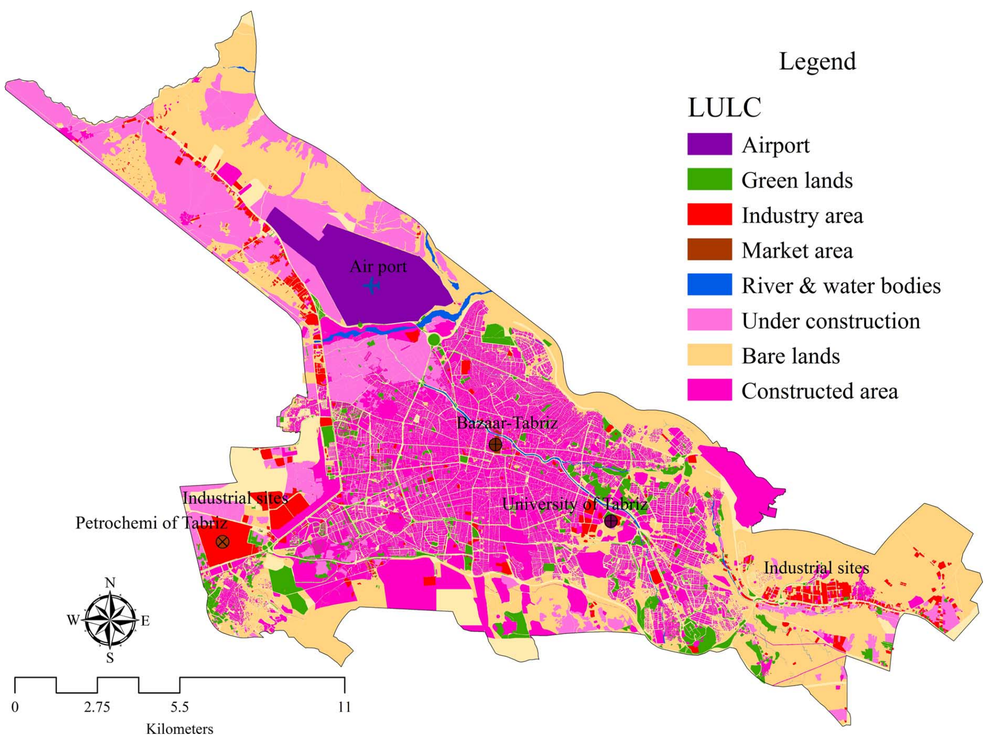

Fig. 3. LULC map of Tabriz city.

IV. Results

A. Relationship of UHI and LULC

The UHI map was compared to a very detailed LULC map of Tabriz city which was derived from aerial photography in a 1:2000 scale, using photogrammetric methods (see Fig. 3). The identified UHI zones were converted to vector format in a GIS environment and integrated with the LULC map (see Fig. 4). In order to analyse the impact of LULC on UHI and their interactions, the relationship between the UHI and LULC maps were investigated. The comparison indicated a positive correlation between HUI, LST and UHI zones which are controlled by LULC classes. A cross-comparison between the UHI map and the LULC map revealed a minimum value of 8.57°C for reflective water bodies. A maximum of 30.34°C was observed for a point in Tabriz petrochemical industrial site. For the LUCL class industry (21.14–29.52°C) the highest LST values fell within construction sites, the market areas of Bazaar-Tabriz and built up areas at the airport. However, moderate temperatures (18–28°C) were also observed within non-vegetated areas

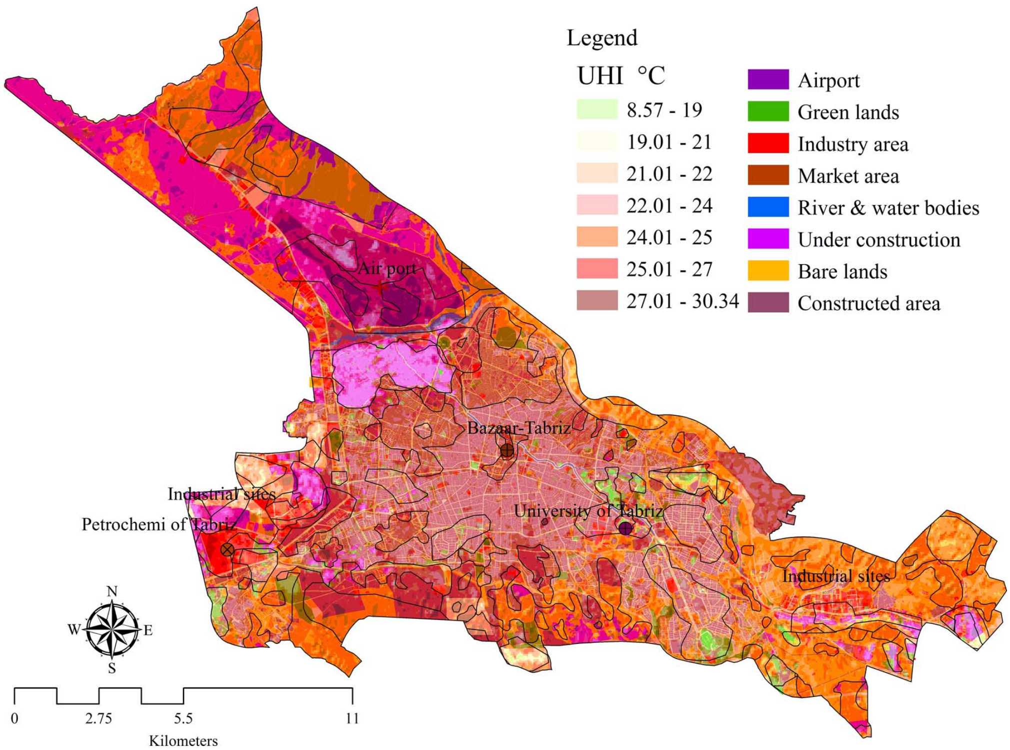

Fig. 4. UHI zones on LULC map of Tabriz city.

(e.g., bare lands and partial residential areas). Further, water bodies and vegetated areas were assigned to the lower temperature categories (8–21°C).

When constructing UHI zones from LST values as described above, the UHI zone with the highest LST value (29.34–30.34°C) was again identified to coincide Tabriz' petrochemical industrial site. The second highest temperature UHI zone with LST values of 22.67–25.76°C was demarcated to be in the bazar market area (Bazaar-Tabriz) in the central part of the city. The third and most widespread UHI zone (LST 19.47–29.52°C) is located in suburbs of Tabriz city and includes a significant amount of bare lands and rock formation. It should also be noted that due to the land use complexity in industrial sites and central parts of the city, the UHI zones in the market areas and industrial sites zones are not extended as widely as the widespread suburb UHI zone. The detailed comparison of UHI and LULC is shown in Table II.

B. Relationship Between UHIs and Air-Pollution Maps

In order to compare UHIs and air-pollution conditions, PM10 values were interpolated as describe in Section III.I. When comparing the PM map to UHI zones a cross-comparison revealed a high correlation between highly air-polluted areas and UHI zones. As Fig. 5 shows, the central part of Tabriz city tends to be highly air-polluted, displaying the highest measured $\mathrm{PM} = 83.99$ values. The UHI zone with a LST of 25–27°C is identified as the highest temperature zone in the central part of the city. However, this UHI zone covers the areas with the highest PM values (see Fig. 5) and therefore the highest air pollution. Based on the PM map, the areas with $\mathrm{PM} > 69$ are located in the central part of Tabriz city, right in the market area of Bazaar-Tabriz. High population density, the high degree of commercial activities of all kinds and the heavy daily traffic account for the high air- pollution in this area. The second important UHI zone with PM values about 55–65 was identified in the industrial

TABLE II
COMPARATIVE RESULTS OF LST AND LUC

LULC class	LST (°C)	Standard Deviation
Industry area including all industrial sites	21.81–30.34	2.132
Constructed area including: residential and built up area	21.14–27.68	1.678
Market area: Bazaar-Tabriz	22.67–25.76	1.683
Under construction: bare lands and the area under construction activities	19.47–29.52	2.441
Airport	18.84–28.61	2. 350
Bare lands including rock formation in suburbs	18.01–28.47	2. 571
Green lands including: parks, gardens and agricultural lands located in city area	17.10–21.90	1. 465
River &water bodies	8.57–12.24	0.632

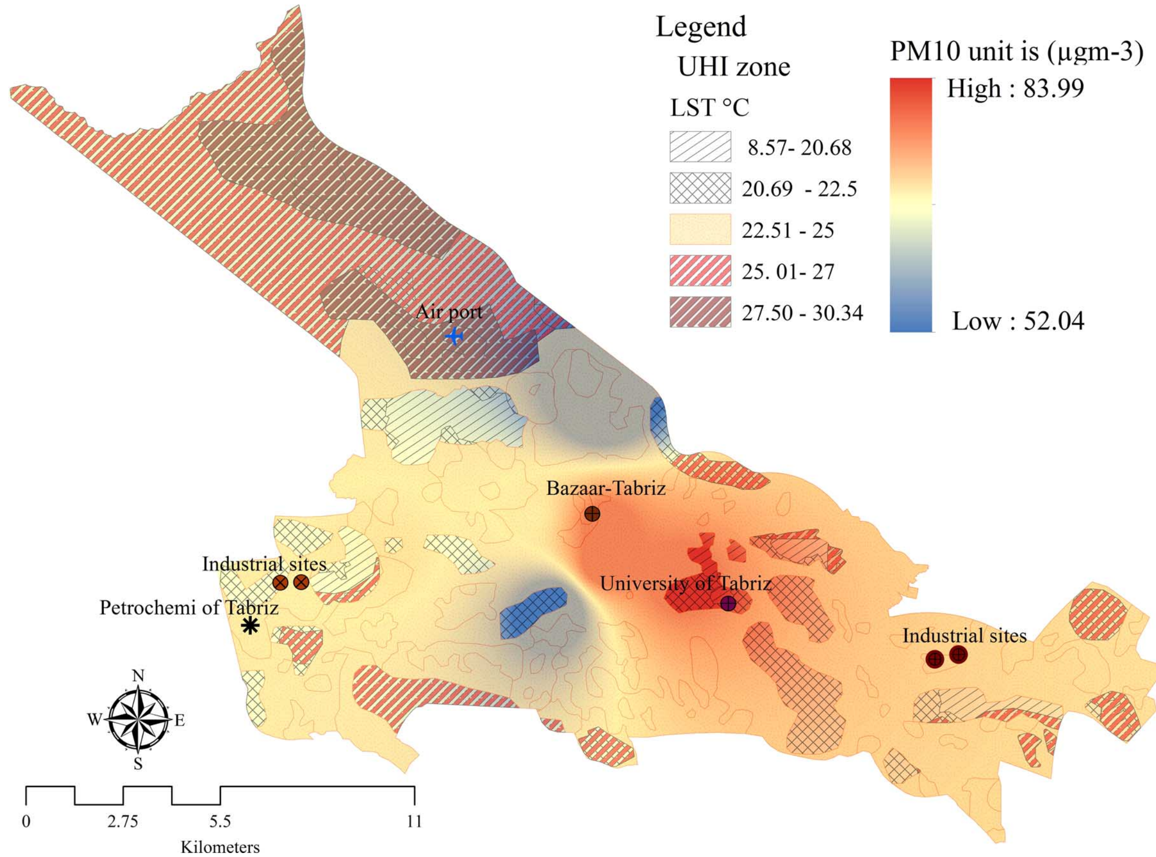

Fig. 5. UHI zones and air pollution map.

sites and in particular within the Tabriz petrochemical site and its neighborhood with a LST of about $< 25°$C. These results clearly demonstrate a high correlation between highly air-polluted areas and the identified UHI zones.

V. Discussion and Conclusion

Our research results confirm a negative correlation between LST and vegetation canopy, as well as moisture, as already known from many other studies. LST was found to be very sensitive to vegetation and humidity. It was also found that UHIs are closely linked to urban LST and LULC. Based on the results of this research, several UHI zones were identified in Tabriz city. The UHI zones with lowest LST were found in water bodies and vegetated areas with LSTs ranging between 8.57–19°C and 19–21°C, respectively. In contrast, UHI zones with high LST were identified in construction zones and industrial sites. However, in the central part of Tabriz city, two UHI zones with LSTs of about 24–25°C and 25.01–27°C were identified in the market area (Bazaar-Tabriz). In terms of air pollution, the highest PM values (>80) were measured in the market area of Bazaar-Tabriz. This is pointed out by the high correlation between UHI and air pollution in Tabriz city. Further, UHI zones with LST $<25°$C were found in industrial sites with relatively high PM values (55–65).

Our results suggest a high correlation between LST, UHI, and air pollution in general. Furthermore, the results reveal several different environmental impact factors of urbanization processes in Tabriz city. Obviously, urbanization transforms the natural land surfaces and increases artificial LULC such as buildings, roads and other impervious surfaces, making urban landscapes fragmented and complex and affecting the inhabitability of cities [18]. Hence, the enormous changes of LULC with encroachment and destruction of the urban green spaces, has led to an increased intensity of UHIs [27]. The rapid urbanization process has brought about many eco-environmental problems, such as the drastic change of land use and the development of UHI [28], [10]. The most imperative problem in urban areas is the increasing surface temperature due to alteration and conversion of vegetated surfaces to impervious surfaces. These changes cause environmental impacts and affect the absorption of solar radiation, surface temperature, evaporation rates, storage of heat, wind turbulence and can drastically alter the conditions of the near-surface atmosphere over the cities [27], [10].

Based on the current rate of pollution growth, for a future 10-year scenario, we assume that urban built-up areas may further increase by the same proportion as in the past 10 years from 2000 to 2010. Thus, further UHI intensity can be predicted by increasing population numbers and the increasing use of fossil fuels in Tabriz city. Since our research results indicate a strong positive correlation between UHI and air pollution, we conclude that an increased intensity in UHI would also mean an increased intensity of air pollution. This may indicate the importance of the results of this research to decision-makers and, in particular, to government departments of the East Azerbaijan Province of Iran. Results will be provided to decision-making authorities in order to take further action to control LULC changes and to control air pollution and UHI intensities.

Acknowledgment

The authors would like to thank the anonymous reviewers for their constructive comments on an earlier version of this paper.

References

[1] M. L. Imhoff, P. Zhang, R. E. Wolfe, and L. Bounoua, "Remote sensing of the urban heat island effect across biomes in the continental USA," *Remote Sens. Environ.*, vol. 114, pp. 504–513, 2010.
[2] B. Feizizadeh and T. Blaschke, "Land suitability analysis for Tabriz County, Iran: A multi-criteria evaluation approach using GIS," *J. Environ. Plan. Manag.*, vol. 56, pp. 1–23, 2013.
[3] R. Amiri, Q. Weng, A. Alimohammadi, and S. K. Alavipana, "Spatial-temporal dynamics of land surface temperature in relation to fractional vegetation cover and land use/cover in the Tabriz urban area, Iran," *Remote Sens. Environ.*, vol. 113, pp. 2606–2617, 2009.
[4] Q. Weng, D. Lu, and J. Schubring, "Estimation of land surface temperature-vegetation abundance relationship for urban heat island studies," *Remote Sens. Environ.*, vol. 89, pp. 467–483, 2004.
[5] Z. Q. Li and Q. G. Zhou, "Utility of Landsat image in the study of land cover and land surface temperature change," *Procedia Environ. Sci.*, vol. 10, pp. 1287–1292, 2011.
[6] C. P. Lo, D. Quattrochi, and J. Luvall, "Application of high-resolution thermal infrared remote sensing and GIS to assess the urban heat island effect," *Int. J. Remote Sens.*, vol. 18, pp. 287–304, 1997.
[7] Q. Weng, "A remote sensing-GIS evaluation of urban expansion and its impact on surface temperature in the Zhujiang Delta, China," *Int. J. Remote Sens.*, vol. 22, no. 10, pp. 1999–2014, 2001.
[8] H. E. Landsberg, *The Urban Climate*. New York, NY, USA: Academic Press, 1981.
[9] B. Feizizadeh, T. Blaschke, H. Nazmfar, E. Akbari, and H. R. Kohbanani, "Monitoring land surface temperature relationship to land use/land cover from satellite imagery in Maraqeh County, Iran," *J. Environ. Plan. Manag.*, 2013, DOI: 10.1080/09640568.2012.717888.
[10] F. Yuan and M. E. Bauer, "Comparison of impervious surface area and normalized difference vegetation index as indicators of surface urban heat island effects in Landsat imagery," *Remote Sens. Environ.*, vol. 106, pp. 375–386, 2007.
[11] J. A. Voogt and T. R. Oke, "Thermal remote sensing of urban climate," *Remote Sens. Environ.*, vol. 86, pp. 370–384, 2003.
[12] B. Feizizadeh and T. Blaschke, "Thermal remote sensing for examining the relationship between urban land surface temperature and land use/cover in Tabriz city, Iran," in *Proc. IEEE IGARSS*, Jul. 2012, pp. 2229–2232, DOI: 10.1109/IGARSS.2012.6351056.
[13] G. Yang, P. Ruiliang, Z. Chunjian, H. Wenjiang, and W. Jihua, "Estimation of subpixel land surface temperature using an endmember index based technique: A case examination on ASTER and MODIS temperature products over a heterogeneous area," *Remote Sens. Environ.*, vol. 115, pp. 1202–1219, 2011.
[14] N. Agam, W. P. Kustas, M. C. Anderson, F. Q. Li, and C. M. U. Neale, "A vegetation index based technique for spatial sharpening of thermal imagery," *Remote Sens. Environ.*, vol. 107, pp. 545–558, 2007.
[15] A. R. Huete, "A soil adjusted vegetation index (SAVI)," *Remote Sens. Environ.*, vol. 25, pp. 295–309, 1998.
[16] D. Lu and Q. Weng, "Spectral mixture analysis of ASTER images for examining the relationship between urban thermal features and biophysical descriptors in Indianapolis, Indiana, USA," *Remote Sens. Environ.*, vol. 104, pp. 157–167, 2006.
[17] M. O. Smith, S. L. Ustin, J. B. Adams, and A. R. Gillespie, "Vegetation in deserts: I. A regional measure of abundance from multispectral images," *Remote Sens. Environ.*, vol. 31, pp. 1–26, 1990.
[18] Q. Weng, U. Rajasekar, and X. Hu, "Modeling urban heat islands and their relationship with impervious surface and vegetation abundance by using ASTER images," *IEEE Trans. Geosci. Remote Sens., Special Issue on IGARSS 2010*, vol. 49, no. 10, pp. 4080–4089, Oct. 2011.
[19] Q. Weng and D. Lu, "Landscape as a continuum: An examination of the urban landscape structures and dynamics of Indianapolis city, 1991–2000," *Int. J. Remote Sens.*, vol. 30, pp. 2547–2577, 2009.
[20] D. A. Roberts, M. Gardner, R. Church, S. Ustin, G. Scheer, and R. O. Green, "Mapping Chaparral in the Santa Monica Mountains using multiple endmember spectral mixture models," *Remote Sens. Environ.*, vol. 65, pp. 267–279, 1998.
[21] K. L. Roth, P. E. Dennison, and D. A. Roberts, "Comparing endmember selection techniques for accurate mapping of plant species and land cover using imaging spectrometer data," *Remote Sens. Environ.*, vol. 127, pp. 139–152, 2012.
[22] F. Li, T. J. Jackson, W. P. Kustas, T. J. Schmugge, A. N. French, and M. H. Cosh, "Deriving land surface temperature from Landsat 5 and 7 during," *Remote Sens. Environ.*, vol. 92, pp. 521–534, 2004.
[23] W. C. Snyder, Z. Wan, Y. Zhang, and Y.-Z. Feng, "Classification-based emissivity for land surface temperature measurement from space," *Int. J. Remote Sens.*, vol. 19, pp. 2753–2774, 1998.
[24] R. Pu, P. Gong, R. Michishita, and T. Sagwa, "Spectral mixture analysis for mapping abundance of urban surface components from the Terra/ASTER data," *Remote Sens. Environ.*, vol. 112, pp. 939–954, 2008.
[25] Z. Mitraka, N. Chrysoulakis, Y. Kamarianakis, P. Partsinevelos, and P. Tsouchlaraki, "Improving the estimation of urban surface emissivity based on sub-pixel classification of high resolution satellite imagery," *Remote Sens. Environ.*, vol. 117, pp. 125–134, 2012.
[26] J. B. Adams, D. E. Sabol, V. Kapos, R. A. Filho, D. A. R. A. Roberts, M. O. Smith, and A. R. Gillespie, "Classification of multispectral images based on fractions of endmembers: Application to land cover change in the Brazilian Amazon," *Remote Sens. Environ.*, vol. 52, pp. 137–154, 1995.
[27] A. S. Mather, *Land Use*. London, U.K.: Longman, 2008.
[28] Y. K. Mallick and B. D. Bharath, "Estimation of land surface temperature over Delhi using Landsat-7 ETM+," *J. Indian Geophys. Union*, vol. 12, no. 3, pp. 131–140, 2008.

Bakhtiar Feizizadeh is currently pursuing the Ph.D. degree within the doctoral program Applied Geoinformatics at the University of Salzburg, Salzburg, Austria. His main research interests include methodological issues in geoinformatics, integration of GIS and Remote Sensing for land use/cover monitoring, land suitability analysis, geohazard and risk assessment, in particular landslide mapping. He has practiced developing methodology for GIS based Multicriteria Decision Anlysis (GIS-MCDA), modelling sensitivity and uncertainty in GIS environment, Object Based Image Analysis (OBIA) and thermal Remote Sensing image processing. He has published more than 50 scientific publications and has teaching experiences in both Remote Sensing and GIS.

Thomas Blaschke is a full Professor at the University of Salzburg and Deputy Chair of the Department of Geoinformatics – Z_GIS, Head of the Research Studio iSPACE and Director of the Doctoral College GIScience. His research interests include methodological issues of the integration of GIS, remote sensing and image processing also with aspects of participation and human-environment interaction. His academic record includes several temporary affiliations as guest professor and visiting scientist in Germany, the UK and the US including a Fulbright Professorship at California State University and has 300 scientific publications including 65 journal publications. He is author, co-author or editor of 17 books and received several academic prices and awards including the Christian-Doppler Prize 1995.